Characterization of homogeneous regions for regional peaks-over-threshold modeling of heavy precipitation

Julie Carreau, Philippe Naveau, Luc Neppel

Characterization of homogeneous regions for regional peaks-over-threshold modeling of heavy precipitation

Julie Carreau[a] Philippe Naveau[b] Luc Neppel[a]

Julie.Carreau@univ-montp2.fr, (phone) +33467149027, (fax) +33467144774

[a] HydroSciences Montpellier, CNRS/IRD/UM, Université de Montpellier - Case 17, 163 rue Auguste Broussonet 34090 Montpellier, France
[b] LSCE, IPSL-CNRS, Orme des Merisiers, Gif-sur-Yvette, France

Abstract

In the French Mediterranean area where heavy precipitation events can yield devastating consequences, it is essential to obtain reliable estimates of the distribution of extreme precipitation at gauged and ungauged locations. Under mild assumptions, extremes defined as excesses over a high enough threshold can be modeled by the generalized Pareto (GP) distribution. The shape parameter of the GP which characterizes the behavior of extreme events is notoriously difficult to estimate. In regional analysis, the sample variability of the shape parameter estimate can be reduced by increasing the sample size. This is achieved by assuming that sites in a so-called homogeneous region are identically distributed apart from a scaling factor and therefore share the same shape parameter. A major difficulty is the proper definition of homogeneous regions. We build upon a recently proposed approach, based on the probability weighted moment (PWM) for the GP distribution, that can be cast into a regional framework for a single homogeneous region. Our main contribution is to extend its applicability to complex regions by characterizing each site with the second PWM of the scaled excesses. We show on synthetic data that this new characterization is successful at identifying the homogeneous regions of the generative model and leads to accurate GP parameter estimates. The proposed framework is applied to 332 daily precipitation stations in the French Mediterranean area which are splitted into homogeneous regions with shape parameter estimates ranging from 0 to 0.3. The uncertainty of the estimators is evaluated with an easy-to-implement spatial block bootstrap.

keywords : regional analysis, probability weighted moment, generalized Pareto distribution, spatial block bootstrap, extreme precipitation, French mediterranean area, clustering

1 Introduction

Flash floods, a sudden rise of the water level (in a few hours or less) together with a significant peak discharge, are the main natural hazard in the French Mediterranean area. They can potentially cause fatalities and important material damage [Borga et al., 2011, Braud et al., 2014]. Flash floods might be triggered by intense rainfall events occurring mainly in the fall [Delrieu et al., 2005]. Therefore, to design infrastructure to mitigate the impacts of these natural hazards, a reliable estimation of the distribution of extreme precipitation events is crucial, both at gauged and ungauged locations.

Extreme value theory [Coles, 2001] provides a sound asymptotic framework to model the distribution of extremes. In particular, the extremal-type theorem [Fisher and Tippett, 1928, Gnedenko, 1943] states that if the distribution of properly re-scaled maxima converges to a nondegenerate distribution, this distribution is the generalized Extreme Value (GEV) distribution. This gives rise to the block maxima approach which consists of fitting the GEV to the maxima extracted from sufficiently large blocks of observations, often taken as years. Moreover, provided that the maxima converge in distribution to the GEV, the distribution of the excesses above a threshold converges to the generalized Pareto (GP) distribution [Balkema and de Haan, 1974, Pickands, 1975]. The so-called peaks-over-threshold (PoT) approach proceeds by setting a sufficiently high threshold and estimating the GP parameters from the excesses above that threshold. The PoT approach is often preferred over the block maxima approach as more observations can be included in the analysis and this might reduce the estimator variance [Roth et al., 2012]. However, Ferreira and de Haan [2015] showed that the block maxima approach can be rather efficient. In both approaches, the shape parameter of the GEV or the GP characterizes the behavior of the upper tail of the distribution that governs the probability of extreme events.

While the block maxima and the PoT approaches require rather long sample and may be employed solely at gauged sites, regional analysis developed a robust framework to estimate the distribution of extreme events at ungauged sites or sites with short record length. In order to increase the sample size at a given target site, extreme events at neighboring sites are assumed to have the same distribution apart from a scaling factor. Regions for which this assumption is valid are termed *homogeneous*. These regions can be either contiguous and form a partition, or overlapping, defined as neighborhoods around each target site as in the region of influence approach [Burn, 1990]. For a given target site, that could be ungauged or with short record length, regional analysis involves the following steps [Hosking and Wallis, 2005]. First, a homogeneous region, to which the target site belongs, must be defined. Second, observations at each gauged site in the homogeneous region are normalized, i.e. divided by the site-specific scaling factor. Then, the regional distribution is fitted to the normalized observations from all the gauged sites in the region. Next, the scaling factor is interpolated (or estimated locally if enough observations are available) at the target site. Return levels are obtained as the product of the return levels of the regional distribution and the scaling factor of the target site.

Combining an extreme-value approach with regional analysis allows to interpolate at ungauged locations and to decrease the uncertainty of the estimation of the shape parameter which is central in assessing the risk of extreme precipitation events. Indeed, to satisfy the homogeneity assumption, the shape parameter has to be constant across the region and the normalized observations from all the sites contribute to the estimation. For instance, Kyselỳ et al. [2011] and Carreau et al. [2013] employed the GEV in a regional analysis of annual maxima of precipitation while Madsen

and Rosbjerg [1997] and Roth et al. [2012] used the GP for threshold excesses. The latter combination leads to the potentially largest increase in sample size. Besides regional analysis, other ways to exploit information of gauged sites that are similar in distribution in order to interpolate or to strengthen the distribution of extreme events have been proposed. For instance, a direct interpolation of the site parameter estimates or a regression model for the GEV of GP parameters either in a frequentist [Blanchet and Lehning, 2010, Ceresetti et al., 2012] or bayesian approach [Cooley et al., 2007, Renard, 2011] have been considered.

As noted in Renard [2011], the identification of homogeneous regions can be seen as a limitation of the regional approach. Indeed, it generally involves several steps some of which call for subjective decisions, see Burn and Goel [2000], Kyselỳ et al. [2007, 2011] for instance. The recommended approach, described in Hosking and Wallis [2005], advocates the use of physiographic variables such as geographical and climatological characteristics to identify the regions. After the initial identification, the regions are tested for homogeneity by resorting to L-Moment ratios. Heteregeneous regions are re-defined until they pass the homogeneity test. An alternative approach to identify homogeneous regions, see for example Durocher et al. [2016] and the references therein, seeks to model the relationship between physiographic variables, available at all sites, and hydrological variables, available only at gauged sites. Additional shortcomings of regional analysis concern (i) the potential invalidity of the scale invariance assumption of the regional distribution which implies that the normalized observations from a given homogeneous region have a constant scale parameter, (ii) the lack of physical reason behind the definition of the scaling factor and (iii) the difficulty to evaluate the uncertainty of the estimators partly as a result of the spatial dependence of the observations [Gupta et al., 1994, Renard, 2011, Van de Vyver, 2012].

In this work, we build on the approach recently proposed in Naveau et al. [2014] to address some of the shortcomings of the regional approach. The Naveau et al. [2014] approach, which rely on probability weighted moments for the GP distribution [Diebolt et al., 2007], can easily be cast into the regional framework with a single homogeneous region. As is the case with L-Moments, probability weighted moments estimates are fast to compute and may serve as starting values to estimation procedures that require an optimization scheme (such as maximum-likelihood or Bayesian estimators). Moreover, the Naveau et al. [2014] approach does not need to enforce the scale invariance assumption of the normalized observations since it is automatically fulfilled thanks to the choice of scaling factor. The main contribution of this paper is to propose a characterization of each site based on probability weighted moments that stems straightforwardly from the Naveau et al. [2014] approach and extends its applicability to complex area with several homogeneous regions. Sites that are characterized with similar values belong to the same homogeneous region. Based on this notion of similarity, homogeneous regions can be identified either as contiguous regions by employing a clustering algorithm or as overlapping regions resulting from neighborhoods around target sites. We focus on the former option and rely on the K-Means algorithm to partition the sites into homogeneous regions. The k-nearest neighbor rule is used to assign ungauged sites to a homogeneous region (see Ripley [1996] for a detailed presentation of both K-means and the k-nearest neighbor rule). Partitions of homogeneous regions associated to risk levels linked to the shape parameters of the regional GP distribution may be useful for operational early warning system such as `http://vigilance.meteofrance.com/`. Lastly, the sampling distribution of the GP parameter estimates of the proposed regional framework, from which uncertainty estimates can be deduced, is obtained with an easy-to-implement spatial block bootstrap.

The article is organised as follows. The precipitation data which motivates this work is presented

in Section 2. We then describe the basic framework, in Section 3, to set up the methodology which is the basis of the regional framework presented in Section 4. The latter contains a simulation study, Section 4.4, and both the basic and the regional framework are applied to the precipitation data, Section 3.4 and 4.5 respectively. In Section 5, results are discussed and some conclusions are drawn.

2 Daily precipitation data

The French Mediterranean area is subject to intense rainfall events which may trigger floods and landslide with dramatic human and material consequences [Delrieu et al., 2005, Braud et al., 2014]. The occurrence of these intense rainfall events and their high spatial variability are due to the combination of the Mediterranean climate with the complex orography of the region.

Daily precipitation at 332 stations over the period 01/01/1958 to 31/12/2014 (57 years) were collected by Météo-France, the French weather service. Stations are located in the French Mediterranean area whose orography can be seen from the digital elevation map in Fig. 1a. The 332 stations are depicted in Fig. 1b. The size of the plotting symbol is proportional to the length of the observation period available (from 10 to 57 years). The color indicates the percentage of missing values over the observation period (from 0% in light orange to 10 % in dark red). The following landmarks are depicted (and will be in the subsequent figures related to the precipitation data) : two contour level curves, 400 m and 800 m, of the digital elevation map in dark and light shades of gray respectively and two cities (Valence and Montpellier).

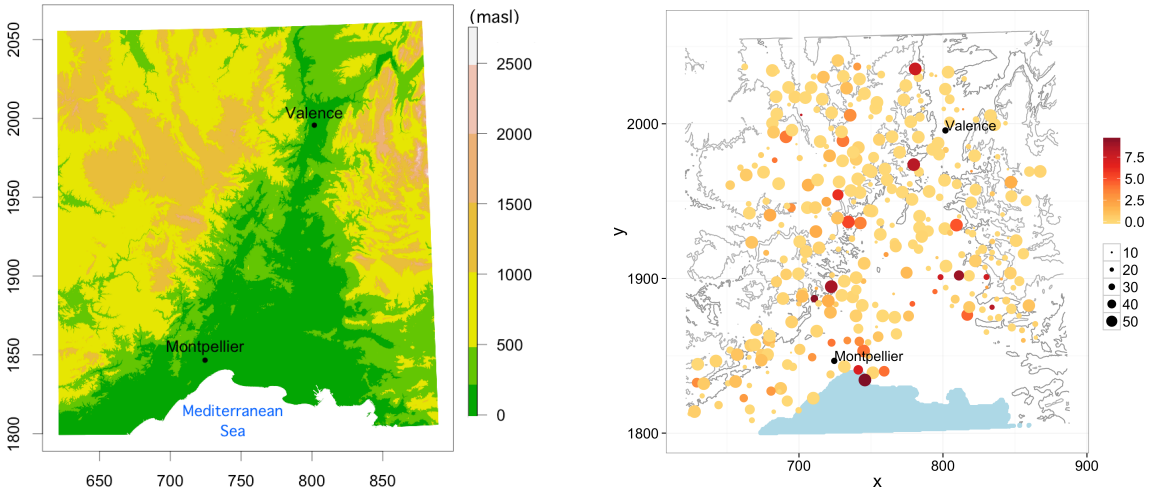

(a) *Digital elevation map* **(b)** *332 rain gauge stations*

Figure 1: *Region of the French Mediterranean area : orography (left) and rain gauge stations (right). In the latter figure, the size of the symbol is proportional to the length of the observation period (10 to 57 years) and the color shade (light orange to dark red) indicates the percentage of missing values (0-10%).*

3 Basic framework

We introduce the following notation. Let the M gauged sites in the region of interest be indexed by i. In addition, let $\boldsymbol{x}$ be a vector of covariates which is available at any site in the region, gauged

or ungauged.

3.1 Kernel regression

In all the approaches developed subsequently, whenever a quantity has to be interpolated, we use kernel regression which is a non-parametric approach [Nadaraya, 1964, Watson, 1964]. The kernel function $K_h(\cdot)$ can be thought of as a symmetric density function for which the so-called *bandwidth* h acts as a scale parameter. The bandwidth controls the amount of smoothing in the interpolation.

More precisely, to interpolate a given quantity $q(\cdot)$ with respects to covariates $\boldsymbol{x}$, we proceed in two steps. First, for each site i, $q(\boldsymbol{x}_i)$ is estimated locally, i.e. based on the observations at site i. Second, the following weighted average corresponds to the interpolated value for the covariates $\boldsymbol{x}$:

$$\tilde{q}(\boldsymbol{x}) = \frac{1}{\sum_i K_h(\boldsymbol{x} - \boldsymbol{x}_i)} \sum_{i=1}^{M} \hat{q}(\boldsymbol{x}_i) K_h(\boldsymbol{x} - \boldsymbol{x}_i) \tag{1}$$

where $\hat{q}(\boldsymbol{x}_i)$ is a local estimate at site i.

We rely on the implementation in the `np` package of `R` [Hayfield and Racine, 2008]. It implements kernel regression with various types of kernels and several automated bandwidth selection methods. We employed the Epanechnikov kernel which is optimal in the sense that it minimizes the asymptotic mean integrated square error [Epanechnikov, 1969, Abadir and Lawford, 2004]. Bandwidth selection is peformed before each spatial interpolation (see Li and Racine [2004] and the documentation in the `np` package [Hayfield and Racine, 2008]).

3.2 Generalized Pareto tail approximation

Under mild assumptions, the generalized Pareto (GP) distribution can be used as an approximation to the upper tail of the distribution of most random variables [Pickands, 1975]. In other words, given a high enough threshold u suitably chosen, the GP distribution approximates the distribution of the excesses over u. Let $Y \sim G(\sigma, \xi)$ be a random variable representing the excesses that follows a GP distribution with scale parameter $\sigma > 0$ and shape parameter $\xi \in \mathbb{R}$. The survival function of Y is provided in Eq. (2) and obey the following domain restrictions : $y \geq 0$ when $\xi \geq 0$ and $y \in [0, -\sigma/\xi)$ when $\xi < 0$. The shape parameter describes the upper tail behavior : heavy (Pareto-type) when $\xi > 0$, light (exponential) when $\xi = 0$ or with a finite upper bound for $\xi < 0$.

$$\mathbb{P}(Y > y) = \overline{G}(y; \sigma, \xi) = 1 - G(y; \sigma, \xi) = \begin{cases} \left(1 + \xi \frac{y}{\sigma}\right)^{-1/\xi} & \text{if } \xi \neq 0 \\ \exp\left(-\frac{y}{\sigma}\right) & \text{if } \xi = 0. \end{cases} \tag{2}$$

High quantiles associated to long return periods such as 100 years are often used by practioners for risk assessment. Let $l(T)$ be the quantile, also termed return level, with a return period of T years, i.e. the level that is exceeded on average once every T years. Thanks to the GP tail approximation, $l(T)$ can be estimated as a quantile of the GP distribution as follows :

$$l(T) = \begin{cases} u + \frac{\sigma}{\xi}((T\ N_{exc})^{\xi} - 1) & \text{if } \xi \neq 0 \\ u + \sigma \log(T\ N_{exc}) & \text{if } \xi = 0 \end{cases} \tag{3}$$

provided that $l(T)$ is greater than the threshold u and where $N_{exc} = 365.25\ \zeta_u$ is the average number of excesses per year with ζ_u the probability of exceeding the threshold u.

3.3 Probability weighted moment estimators

We develop expressions to estimate the parameters of the GP distribution based on the probability weighted moments. The introduction of a normalized variable Z enables a straightforward extension to the framework of regional analysis.

For $r \geq 0$, the probability weighted moments for the GP distribution are given by [Diebolt et al., 2007] :

$$\mathbb{E}[Y\overline{G}(Y;\sigma,\xi)^r] = \sigma\frac{1}{(1+r)(1+r-\xi)}. \tag{4}$$

Sample estimates can be computed using U-statistics, see Furrer and Naveau [2007]. In particular, if $\xi < 1$, the first probability weighted moment, obtained with $r = 0$ in Eq. (4), is the expectation of Y and can be written as :

$$\mu = \mathbb{E}[Y] = \frac{\sigma}{1-\xi}. \tag{5}$$

We consider μ as the scaling factor. In other words, let $Z = {}^{Y}/_{\mu}$ be the normalized variable. Since $\mathbb{P}(Z > z) = \mathbb{P}(Y > \mu\ z) = \mathbb{P}(Y > {}^{(\sigma z)}/_{(1-\xi)})$, where the last equality follows by making use of Eq. (5), we have, by replacing y with ${}^{(\sigma z)}/_{(1-\xi)}$ in Eq. (2), that $Z \sim G(1-\xi,\xi)$. Therefore, the normalized variable Z only depends on the shape parameter ξ.

Let ν be the second probability weighted moment of Z obtained by plugging $\sigma = 1-\xi$ and $r = 1$ in Eq. (4) :

$$\nu = \frac{1-\xi}{4-2\xi}. \tag{6}$$

To estimate the shape parameter of the GP distribution, we then replace ν by its estimator and solve for ξ :

$$\hat{\xi} = \frac{1-4\hat{\nu}}{1-2\hat{\nu}}. \tag{7}$$

The scale parameter is estimated by solving Eq. (5) for σ and replacing μ and ξ by their sample estimates $\hat{\mu}$ and $\hat{\xi}$ respectively :

$$\hat{\sigma} = \hat{\mu}(1-\hat{\xi}). \tag{8}$$

Eq. (7) and (8) are used to estimate the shape and scale parameters in the basic and the regional framework developed in Section 4. In the former, the sample with which the shape parameter is estimated is formed only from the normalized observations from the target site. In the latter, the sample can include normalized observations from all the sites in the homogeneous neighborhood of the target site.

3.4 Preliminary analysis of the daily precipitation data

We apply the basic framework to the French Mediterranean precipitation data described in Section 2. We set up a regular grid (approximately 500 m) covering the region where the stations lie on which the interpolation is carried out. For this application, $M = 332$, the number of gauged sites, and $\boldsymbol{x}$ is taken as the x and y coordinates (extended Lambert II projections of latitude and longitude).

The threshold that defines the excesses for which the GP tail approximation is used is set to the 98% quantile of the precipitation intensities, i.e. the observations greater than 0.1 mm (the sensitivity of daily rain gauges). The threshold and the average number of excesses per year, see Section 3.2, are computed at each station resulting in an overall number of excesses per station ranging from 20 to 191. Local GP parameter estimates are obtained thanks to Eqs. (7-8).

All four local estimates (threshold, average number of excesses per year and shape and scale parameters) are interpolated with kernel regression, see Section 3.1, onto the regular grid, see Fig 2a-2d. The interpolated threshold and average number of excesses define the tail approximation of the GP and will be used also when the regional framework introduced in Section 4 is applied to the French Mediterranean precipitation data. The interpolated shape and scale parameters of the GP will be compared with the estimates from the regional framework.

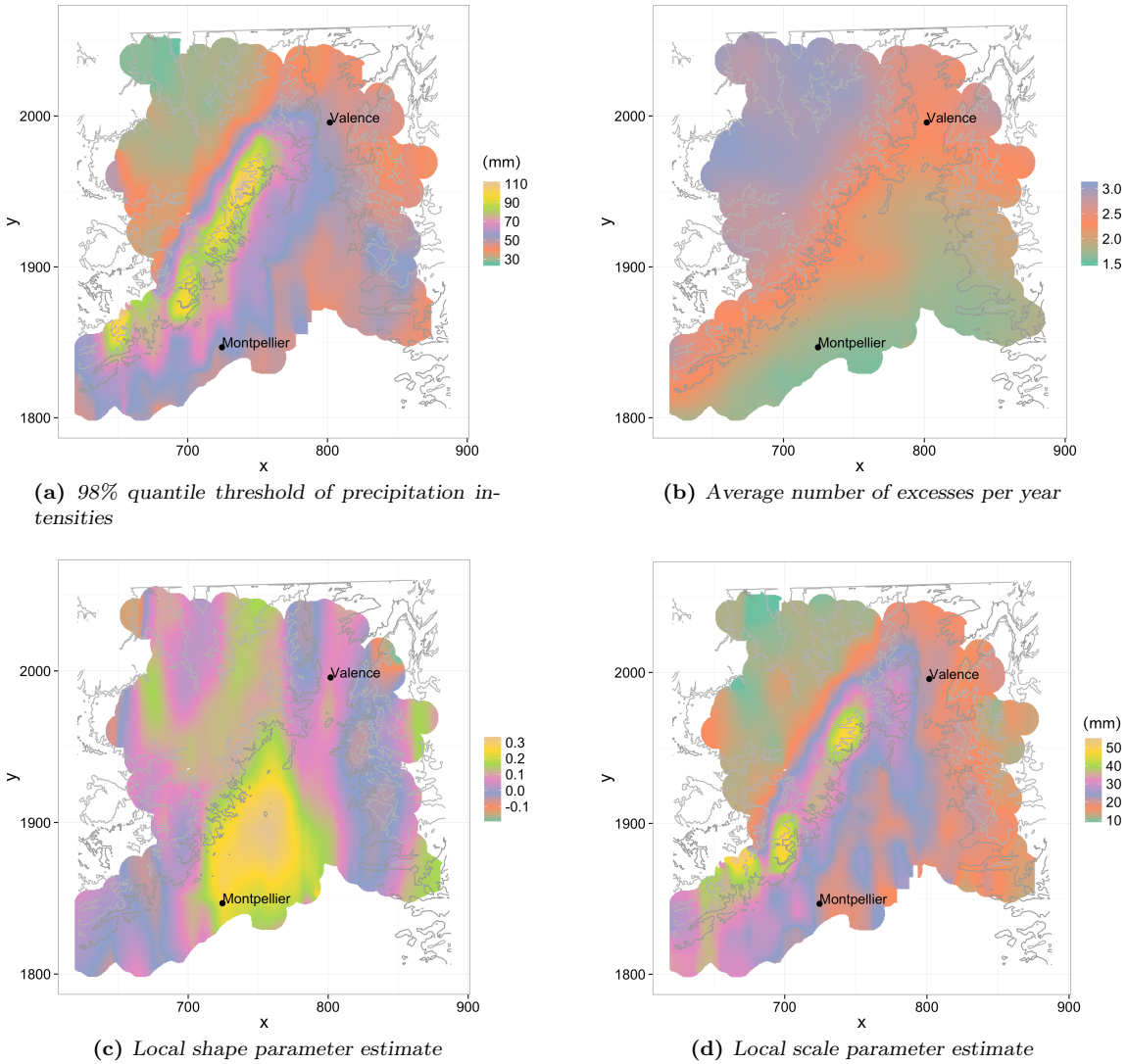

(a) *98% quantile threshold of precipitation intensities*

(b) *Average number of excesses per year*

(c) *Local shape parameter estimate*

(d) *Local scale parameter estimate*

Figure 2: *Application of the basic framework to the French Mediterranean precipitation data. The threshold and resulting average number of excesses per year together with the GP shape and scale parameters are estimated locally and then interpolated with kernel regression.*

4 Regional framework

4.1 Single homogeneous region

We apply the expressions in Section 3.3 to the estimation of the GP parameters in the regional framework stemming from the Naveau et al. [2014] approach with a single homogeneous region, i.e. all the sites belong to the same homogeneous region.

In this work, a region is called homogeneous if the shape parameter is constant over the region and the scale parameter varies smoothly spatially as a function of a vector of covariates $\boldsymbol{x}$. In other words, for a given site i, the distribution of the excesses is given as :

$$Y_i \sim G(\sigma(\boldsymbol{x}_i), \xi), \tag{9}$$

where ξ can be thought of as a *regional* shape parameter. As a result, the scaling factor, that is the expectation of Y_i, also varies spatially since, from Eq. (5), $\mu(\boldsymbol{x}_i) = {}^{\sigma(\boldsymbol{x}_i)}/_{(1-\xi)}$.

Although the scaling factor varies spatially, the normalized variable $Z_i = {}^{Y_i}/_{\mu(\boldsymbol{x}_i)}$ is identically distributed over the region. Indeed, for all i, $Z_i \sim G(1-\xi, \xi)$, i.e. the normalized variable only depends on the regional shape parameter ξ, as in the basic framework in Section 3.3. By construction, the regional shape parameter is constant over the region. It follows that the scale parameter of the normalized variable is also constant. Therefore, the scale invariance assumption, mentioned in the introduction, is automatically fulfilled without any further assumptions on the scale parameter.

The observed excesses from all the sites in the region, once normalized by their expectation, can be used to estimate the regional shape parameter with Eq. (7). Hence, as in the classical regional approach, the sample variability of the estimator of the shape parameter is reduced thanks to an increased sample size. The scale parameter is estimated as before with Eq. (8).

The approach described in this section is related to the work in Naveau et al. [2014] but differs in two main respects. First, they considered $\sigma(\boldsymbol{x}_i)$ as the scaling factor instead of $\mu(\boldsymbol{x}_i)$ which implies that $Z \sim G(1, \xi)$. However, in such a case Z is not observable because $\sigma(\boldsymbol{x}_i)$ is unknown. To circumvent this problem, Naveau et al. [2014] normalized the observations with $\mu(\boldsymbol{x}_i)$ and account for the difference between $\sigma(\boldsymbol{x}_i)$ and $\mu(\boldsymbol{x}_i)$ in their estimators of the GP parameters. Second, in Naveau et al. [2014], both the second and the third probability weighted moments are employed in the estimators. In this work, we adopt right away $\mu(\boldsymbol{x}_i)$ as the scaling factor and use only the second probability weighted moment of the normalized variable Z to estimate ξ. These choices lead to simpler expressions.

4.2 Characterization of homogeneous regions

As can be seen from the local estimation of the shape parameter in the basic framework in Fig. 2c, the assumption of constant shape parameter and thus, of a single homogeneous region, is not reasonable for the French Mediterranean precipitation application. Building on the expressions in Section 4.1, we introduce a characterization of each site with which homogeneous regions can be defined. We partition the sites into N_{reg} contiguous regions, i.e. each site belongs to one region. The so-called "region of influence" approach [Burn, 1990] could also be used as discussed in Section 5.

Let $C_i \in \{1, \ldots, N_{reg}\}$ be the homogeneous region label associated to site i and let $\{\xi_1, \ldots, \xi_{N_{reg}}\}$

be the regional shape parameter associated to each homogeneous region. For a site i belonging to the region C_i, $Y_i \sim G(\sigma(\boldsymbol{x}_i), \xi_{C_i})$ and $Z_i \sim G(1-\xi_{C_i}, \xi_{C_i})$. The regional shape parameter ξ_{C_i} and hence the tail behavior of Y_i varies according to the region C_i. The higher the regional shape parameter is, the greater the risk of extreme precipitation events in the region.

Since the normalized variable only depends on the regional shape parameter, we propose to characterize the site i with a statistic of Z_i. In this work, we choose to use ν, the second probability weighted moment of the normalized variable Z_i, see Eq. (6), to summarize the information on the tail behavior of a given site i. We have that $\nu(\boldsymbol{x}_i) = \nu(\boldsymbol{x}_j)$ if and only if $C_i = C_j$. For each site i, let $\hat{\nu}(\boldsymbol{x}_i)$ be the estimation of ν. This characteristic can be fed to a clustering algorithm to identify the homogeneous regions. In this work, we resort to K-Means to perform the clustering [Ripley, 1996]. K-Means iteratively assigns a site i to the cluster whose cluster center is closer in terms of $\hat{\nu}(\boldsymbol{x}_i)$ and then re-computes the cluster centers as the averages of the $\hat{\nu}(\boldsymbol{x}_i)$ of the sites belonging to each cluster. We set the initial cluster centers to N_{reg} empirical quantiles of $\hat{\nu}(\boldsymbol{x}_i)$, $1 \leq i \leq M$, with probabilities that spread regularly the $[0, 1]$ interval. This ensures that K-Means always converges to the same partition.

4.3 Estimation at ungauged sites

To estimate the GP parameters at an ungauged site i^*, we must first determine to which homogeneous region it belongs. This is a classification problem and we employ the k-nearest neighbor rule with $k = 5$, a non-parametric classifier [Ripley, 1996]. This classifier determines the five nearest neighbors of i^* by evaluating the Euclidean distances $d(\boldsymbol{x}_{i^*}, \boldsymbol{x}_i)$ for all $i \in \{1, \ldots, M\}$ and assigns i^* to a class C_{i^*} by taking a majority vote among its five nearest neighbors. The regional shape parameter at the site i^* is given by $\xi_{C_{i^*}}$ and is estimated as explained in Section 4.1.

To estimate the scale parameter at site i^*, the scaling factor $\mu(\boldsymbol{x}_{i^*})$ is interpolated as in the classical regional approach. It is then combined with the regional shape parameter estimate in Eq. (8).

4.4 Simulation study

We illustrate the regional framework described in this section on synthetic data whose generative model satisfies the assumptions of the framework. The synthetic dataset is a variant, with four homogeneous regions, of the dataset proposed in Naveau et al. [2014] which consists of a single homogeneous region. The one-dimensional covariate x takes value in the interval $[1, 1000]$ that is splitted into four equal sub-intervals : $\xi_1 = 0.3$ when $x \in [1, 250]$, $\xi_2 = 0.2$ when $x \in [251, 500]$, $\xi_3 = 0.1$ when $x \in [501, 750]$ and $\xi_4 = 0$ when $x \in [751, 1000]$. The scale parameter varies with x as a combination of a periodic and exponential signal. Fig. 3a shows a sample from the synthetic dataset with $M = 1000$ sites, $x_i = i$ for $i \in \{1, \ldots, M\}$ and $n_i = 100$ GP samples generated from each Y_i. In Fig. 3a, the scale parameter is depicted as the cyan curve and the homogeneous regions are indicated by the vertical bands.

A detailed description of the regional framework proposed in this paper is given in Algorithm 1. The algorithm must be provided with the following inputs : the number of homogeneous regions N_{reg} and for each site $1 \leq i \leq M$, the n_i observed excesses $\boldsymbol{y}_i = \{y_{i1}, \ldots, y_{in_i}\}$ and the vector of covariates $\boldsymbol{x}_i$. It is possible to provide additional vectors of covariates $\boldsymbol{x}_{i^*}$ corresponding to ungauged sites $1 \leq i^* \leq M^*$. The outputs of the algorithm are the N_{reg} regional shape parameter estimates $\hat{\xi}_j$, $1 \leq j \leq N_{reg}$, the scale parameter estimates $\hat{\sigma}(\boldsymbol{x}_i)$ and the region labels C_i for each

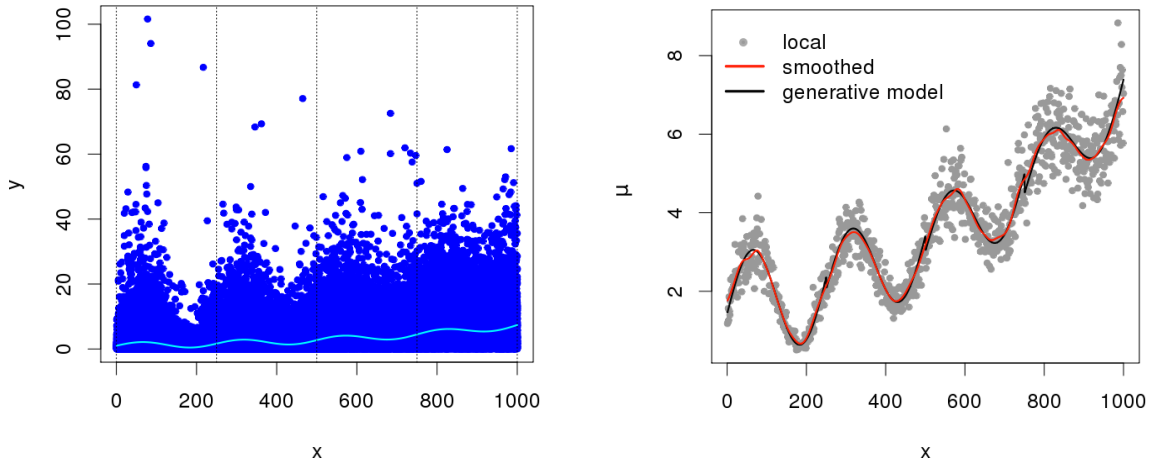

(a) *Synthetic dataset* **(b)** *Estimation of* $\mu(\cdot)$

Figure 3: *Left panel : A GP random sample is simulated in the interval* $[1, 1000]$ *for 1000 sites with covariates taking value* $x = 1, \ldots, 1000$*. The scale parameter varies as a combination of periodic and exponential signal (cyan curve) and the regional shape parameter is piecewise constant decreasing from 0.3, 0.2, 0.1 to 0 in each of the vertical bands. The sample size at each site is* $n_i = 100$*. Right panel : At each* x*, a local estimate* $\hat{\mu}_i$ *of* μ *is computed (gray dots) and then smoothed with kernel regression to obtain* $\hat{\mu}(\cdot)$ *(red curve). The generative model of* $\mu(\cdot)$ *is represented by the black curve.*

site $1 \leq i \leq M$. If additional target sites are included in the inputs, the algorithm returns their region labels and their scale parameter estimates as well. In the synthetic data application, there is no ungauged site estimation. We set the number of regions to the value of the generative model, that is $N_{reg} = 4$.

The first step of the regional framework proposed in this paper consists in estimating the scaling factor (Fig. 3b) and computing the normalized observations (Fig 4a). This corresponds in Algorithm 1 to lines 1 and 2 respectively. Kernel regression is applied to local estimates $\hat{\mu}_i = {}^1/_{n_i} \sum_{k=1}^{n_i} y_{ik}$ to obtain a smooth estimate of $\mu(\cdot)$ (line 1). Then, the excesses at each site i are normalized with the estimated $\hat{\mu}(\cdot)$ yielding $z_{ik} = {}^{y_{ik}}/_{\hat{\mu}(\boldsymbol{x}_i)}$ for $1 \leq k \leq n_i$ (line 2). In Fig. 3b, the scaling factor of the synthetic data example is represented. The gray dots are the local estimates $\hat{\mu}_i$, the red curve represents the kernel regression estimate $\hat{\mu}(\cdot)$ and the generative function $\mu(\cdot)$ is shown in black. In this example, the $\mu(\cdot)$ function of the generative model has discontinuites at the borders of the homogeneous regions and these cannot be well captured by kernel regression. Fig 4a illustrates the normalized sample.

In the second step of the proposed framework, the gauged and ungauged sites are assigned to a homogeneous region (Fig. 4b). If a single homogeneous region is requested, all the M gauged sites and the M^* ungauged sites are pooled together (line 3 of Algorithm 1). Otherwise, the sites are partitioned into N_{reg} regions (line 5). The partitioning goes as follows. Similarly as for $\mu(\cdot)$, $\nu(\cdot)$ is estimated (line 6) by applying kernel regression to the local estimates ν_i computed from z_{ik}, $1 \leq k \leq n_i$ with U-statistics [Furrer and Naveau, 2007]. Then, the M gauged sites are clustered into N_{reg} regions with K-Means based on $\hat{\nu}(\boldsymbol{x}_i)$ (line 7). If ungauged sites are provided as well, they are assigned to a homogeneous region C_{i^*} for each i^* with a k-nearest neighbor classifier with $k = 5$ (line 8). For the synthetic data application, Fig. 4b shows the ν_i as gray dots, the regressed $\hat{\nu}(\cdot)$ as colored curves and the function from the generative model $\nu(\cdot)$ in black (piecewise constant). Each color of the $\hat{\nu}(\cdot)$ curve indicates a cluster and hence an homogeneous region with constant

Algorithm 1: Regional framework for peaks-over-threshold based on the probability weighted moments with a variable number of homogeneous regions with constant shape parameter

input : N_{reg} the number of homogeneous regions ;
$\boldsymbol{y}_i = \{y_{i1}, \ldots, y_{in_i}\}$, n_i observed excesses and $\boldsymbol{x}_i$ a vector of covariates at sites $1 \leq i \leq M$;
$\boldsymbol{x}_{i^*}$ $1 \leq i^* \leq M^*$ for ungauged sites (optional)
output: $\{\hat{\xi}_1, \ldots, \hat{\xi}_{N_{reg}}\}$, $\hat{\sigma}(\boldsymbol{x}_i)$ and C_i for $1 \leq i \leq M$;
C_{i^*} and $\hat{\sigma}(\boldsymbol{x}_{i^*})$ for $1 \leq i^* \leq M^*$

1 Estimate $\mu(\cdot)$ by regressing $\hat{\mu}_i = {}^1/_{n_i} \sum_{k=1}^{n_i} y_{ik}$ over $\boldsymbol{x}_i$;
2 Compute the normalized excesses $z_{ik} = {}^{y_{ik}}/_{\hat{\mu}(\boldsymbol{x}_i)}$ for $1 \leq k \leq n_i$;
3 **if** $N_{reg} == 1$ **then** `// single homogeneous region case`
4 | Assign all the sites to a single region $C_i = 1$ $\forall i$ and $C_{i^*} = 1$ $\forall i^*$;
5 **else** `// partitioning into` N_{reg} `regions`
6 | Estimate $\nu(\cdot)$ by regressing $\hat{\nu}_i$, the second probability weighted moment sample estimate of Z_i, over $\boldsymbol{x}_i$;
| `//` ν_i `is estimated using U-statistics [Furrer and Naveau, 2007]`
7 | Assign each site i to a region C_i, $1 \leq C_i \leq, N_{reg}$ by clustering $\hat{\nu}(\boldsymbol{x}_i)$;
8 | Assign each i^* to a region C_{i^*} with a classifier based on $\boldsymbol{x}_{i^*}$ and $\boldsymbol{x}_i$;
9 **end**
10 **for** $j \leftarrow 1$ **to** N_{reg} **do**
11 | Estimate ν_j from all z_{ik}, $1 \leq k \leq n_i$, such that $C_i = j$;
12 | Estimate ξ_j, the shape parameter of region j as $\hat{\xi}_j = {}^{(1-4\hat{\nu}_j)}/_{(1-2\hat{\nu}_j)}$, see Eq. (7) ;
13 **end**
14 Estimate $\sigma(\boldsymbol{x}_i)$ thanks to $\hat{\sigma}(\boldsymbol{x}_i) = \hat{\mu}(\boldsymbol{x}_i)(1 - \hat{\xi}_{C_i})$, see Eq. (8) ;
15 Estimate $\sigma(\boldsymbol{x}_{i^*})$ similarly ;

shape parameter.

In the last step of the regional framework described in Algorithm 1, the GP parameters are estimated at the gauged and ungauged sites (Fig. 5a and 5b, lines 10 to 15 of Algorithm 1). For each homogeneous region $j \in \{1, \ldots, N_{reg}\}$, all the z_{ik}, $1 \leq k \leq n_i$, belonging to that region, i.e. such that $C_i = j$, serve to estimate ν_j, the regional second probability weighted moment, and ξ_j, the regional shape parameter with Eq. (7) (lines 11-12). Finally, the scale parameter is computed by combining the $\hat{\mu}(\boldsymbol{x}_i)$ estimate (line 1) at the gauged sites $1 \leq i \leq M$ with the regional shape parameter estimate $\hat{\xi}_{C_i}$ of the associated homogeneous region in Eq. (8) (line 14). The same computation is carried out for ungauged sites if needed (line 15). Parametric bootstrap is employed to deduce 95% confidence intervals for the shape and scale estimators of the proposed regional framework (Fig. 5a and 5b respectively). A 1000 copies of the synthetic data set are generated and the estimation at all $M = 1000$ sites is performed on each copy. In Fig. 5a and 5b, the 95 % confidence intervals are shown as gray bands and the parameters of the generative model are shown as black curves.

The main contribution of this work is the use, in the regional framework stemming from the Naveau et al. [2014] framework, of the statistic $\hat{\nu}(\boldsymbol{x}_i)$ that is successful at identifying regions with constant shape parameter, as shown in Fig. 4b. As a consequence, the proposed framework yields a reliable estimation of the shape parameter in each region (see Fig. 5a), provided that the assumptions behind the framework are fulfilled. In addition, by relying on non-parameteric regression instead of local estimation for both μ and ν, spatial information is introduced and the noise of the local estimates is considerably reduced (see Fig. 3b and 4b). Finally, the 95% confidence intervals shows the stability of the algorithm for the synthetic data example and good

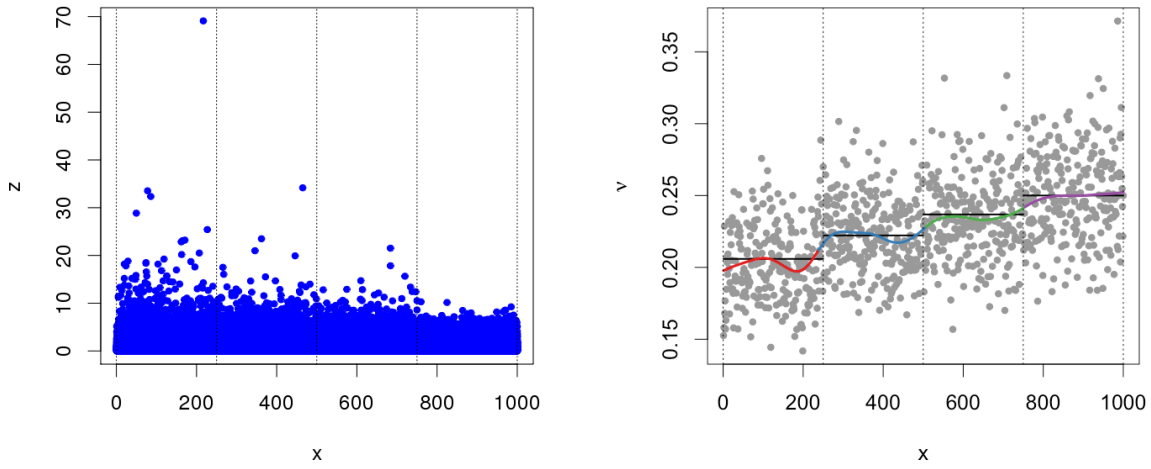

(a) *Normalized sample* $z_{ik} = y_{ik}/\hat{\mu}(\boldsymbol{x}_i)$

(b) *Estimation of* $\nu(\cdot)$ *and partitioning into homogeneous regions*

Figure 4: *Left panel : The synthetic dataset from Fig 3a is normalized with the smoothed* $\hat{\mu}(\cdot)$ *estimate (red curve in Fig. 3b). Right panel : Local estimates* ν_i *are obtained from the normalized sample (gray dots) and kernel regression is applied to obtain a smooth estimate* $\hat{\nu}(\cdot)$ *(colored curves). Homogeneous regions are determined by applying K-Means on the smoothed estimates* $\hat{\nu}(\boldsymbol{x}_i)$*. Each region, represented by a different colored* $\hat{\nu}(\cdot)$ *curve, determines an area with constant shape parameter.*

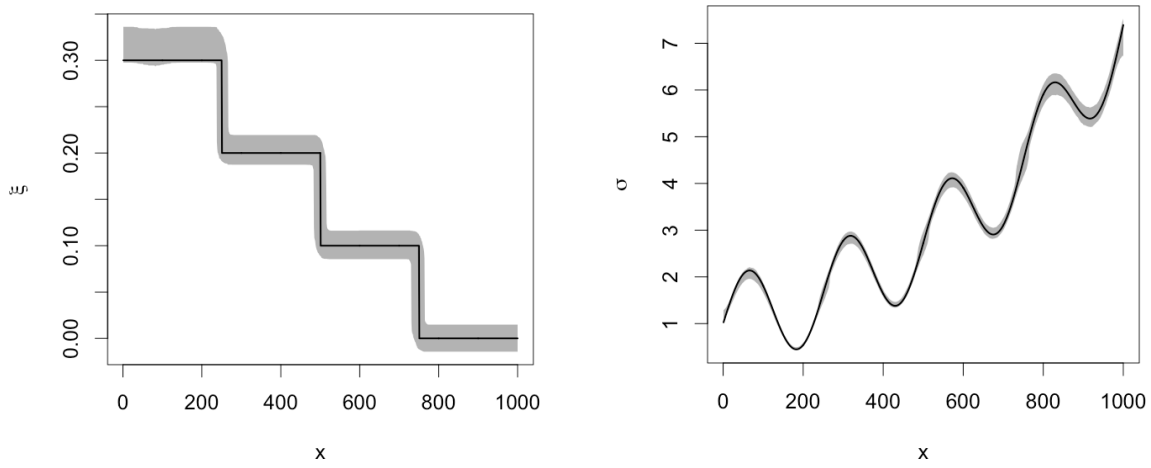

(a) *Shape parameter*

(b) *Scale parameter*

Figure 5: *GP parameter estimates from the regional framework described in Algorithm 1 together with 95% confidence bands computed with parametric boostrap. The black curve represents the generative model. The normalized sample (Fig 4a) is used to estimate the shape parameter within each homogeneous region. The scale parameter estimate is obtained by combining the shape parameter estimate with the smoothed* $\hat{\mu}(\cdot)$ *estimate from Fig. 3b.*

agreement between the estimated and the generative models. Only in the case of the sub-interval corresponding to the higher shape parameter ($\xi_1 = 0.3$), the shape parameter of the generative model is at the lower end of the asymmetric confidence bands.

4.5 Regional analysis of the daily precipitation data

We apply the regional framework described above to the 332 French Mediterranean precipitation stations from Section 2 and compare the results with those from the basic framework in Section 3.4. The same covariates $\boldsymbol{x}$ (the x and y coordinate in extended Lambert II projections of latitude and longitude) and the same regular grid of about 500 m is used for the interpolation. The grid boxes are provided as ungauged sites in Algorithm 1. The threshold that defines the excesses which are approximately GP distributed, along with the corresponding average number of excesses per year, are the same as those presented in the basic framework, see Fig. 2a-2b.

4.5.1 Partitioning into homogeneous regions

From the regional framework of Algorithm 1, a partition into homogeneous regions is obtained as each grid box is assigned to a region corresponding to a regional shape parameter. We present the partitioning for increasing numbers of regions (three to six), sees Fig. 6a-6d. This partitioning can be compared to the estimated shape parameter from the basic framework, see Fig. 2c.

The homogeneous regions are remarkably continuous in space although geographical information is used only indirectly to define the regions through the regression of the local ν_i estimates (line 6 of Algorithm 1). Even in the 6-region partition in Fig. 6d, i.e with the larger number of regions, although the regional parameter estimates can be very similar for some regions, the regions remain approximately spatially coherent. In addition, for all the partitions, the regions are roughly aligned along the same direction, with a slight counterclockwise angle from 12 o'clock (a central vertical line).

In most cases, the regions have clear borders. However, in a number of cases, especially when the number of regions increases, the borders are somewhat blurred. This happens when a region has only a few scattered representative stations in a given geographical area. In such a configuration, the k-nearest neighbor rule yields unstable region assignment.

As the number of regions increases, the partitioning provides more detailed patterns that are nested into the smoother patterns of partitions with less regions. As expected, with a larger number of regions, the partitioning reproduces more closely the patterns of the local estimates in Fig. 2c. On the contrary, with less regions, the shape parameter estimates seem to smooth the local estimates over the larger regions.

For all partitions, the high risk region, corresponding to the highest shape parameter value with $\hat{\xi}_j \approx 0.27 - 0.30$, is located in the South and represented with the blue-green color. The region starts at the coast, goes up to the foothills of the Cevennes mountain range and is consistent with the local estimates in Fig. 2c and expert knowledge [Delrieu et al., 2005, Braud et al., 2014].

4.5.2 Scale parameter estimates

Fig. 7a and 7b present the maps of the differences between the estimated scale parameter from the basic framework, see Fig. 2d, and the estimated scale parameter from the regional framework described in Algorithm 1. The latter estimate corresponds to the partitioning into three and six

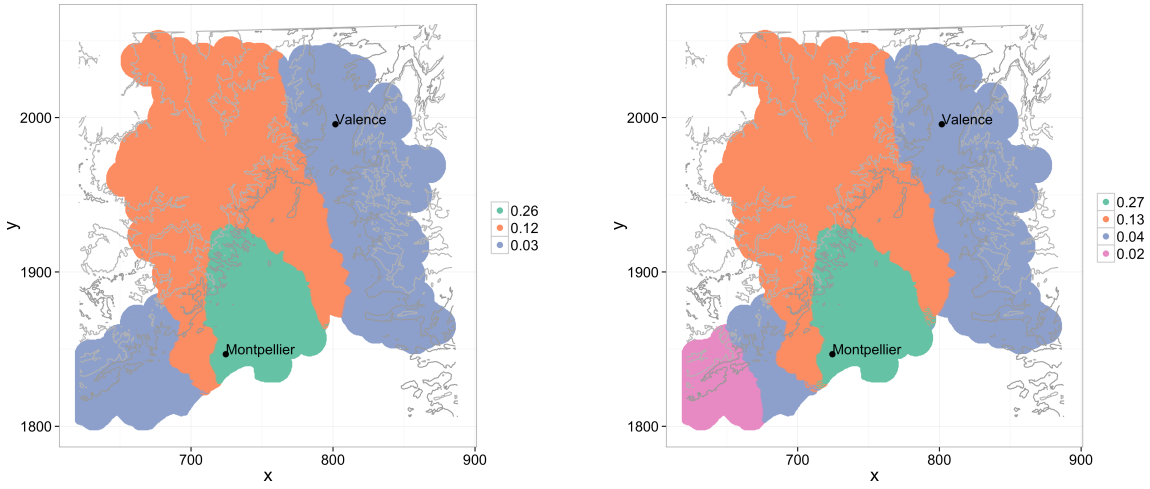

(a) *Three homogeneous regions* **(b)** *Four homogeneous regions*

(c) *Five homogeneous regions* **(d)** *Six homogeneous regions*

Figure 6: *Partitioning into homogeneous regions associated to estimated regional shape parameter values* $\{\hat{\xi}_1, ..., \hat{\xi}_{N_{reg}}\}$ *in the legends. The partitions, with* $N_{reg} = 3, 4, 5, 6$*, are defined based on the regional framework detailed in Algorithm 1.*

regions shown in Fig. 6a and 6d. The results are similar for the partitioning into four and five regions (not shown).

The estimation of the scale parameter with the proposed regional framework is little sensitive to the selected number of regions and is very close to the estimate from the basic framework. Indeed, for all the partitions considered (three to six regions), the differences in scale parameter estimates for about 95% of the grid boxes is at most 5 mm in magnitude.

In most cases, the scale parameter estimates of the proposed regional framework do not show major discontinuities at the region borders. The highest risk region discussed above is an exception : the North-East border is quite visible in the maps of differences in scale parameter estimates Fig. 7a and 7b (this can be compared to the corresponding partitions in Fig. 6a and 6d).

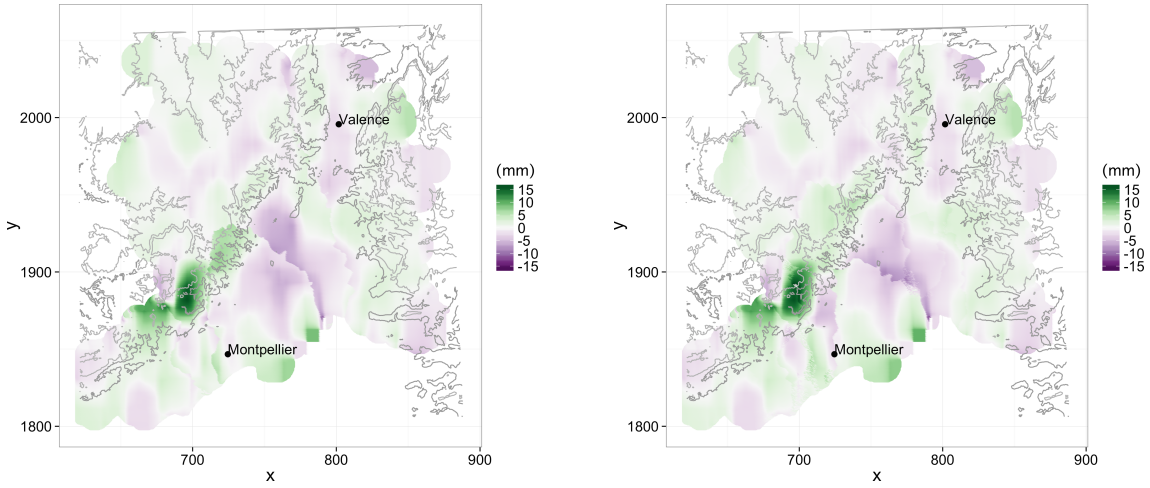

(a) *Three homogeneous regions* **(b)** *Six homogeneous regions*

Figure 7: *Differences in scale parameter estimates : basic framework estimates minus regional framework estimates. In the latter,* $\sigma(\boldsymbol{x}) = \mu(\boldsymbol{x})\ (1 - \xi_j)$ *where* ξ_j *is the regional shape parameter for the* j^{th} *homogeneous region and* $\mu(\boldsymbol{x})]$ *is the conditional expectation of the excesses for the covariates* $\boldsymbol{x}$*. The homogeneous regions corresponds to the partitioning in Fig. 6a and 6d.*

4.5.3 Confidence intervals

We selected two distinctive grid boxes as target sites to illustrate the sampling distributions of the estimators in both the basic and the regional framework. The first grid box is located 20 km East of the city of Montpellier in the high risk region with shape parameter taking value from 0.27 to 0.30, see Fig. 6. In contrast, the second grid box lies 20 km North of the city of Valence in a low risk region with shape parameter value around zero.

The sampling distributions of the GP parameter estimates can be obtained with spatial block bootstrap to preserve temporal and spatial dependence of the excesses. More precisely, blocks of three days are randomly sampled from the original observations for all the stations simultaneously. The size of the block was determined from the maximum number of consecutive excesses in the precipitation data.

The region labels C_i for each gauged site are determined once and for all on the original observations. This means that the configuration of the regions is kept fixed for each bootstrap sample. In addition, the thresholds are estimated only once on the original observations. For

each bootstrap sample, for each site, the excesses are extracted and the scaling factor $\mu(\cdot)$, the conditional estimation of the excesses, is estimated. The normalized observations z_{ik}, $1 \leq k \leq n_i$, are then computed and serve to estimate the regional shape parameters using the original region labels C_i. Last, the scale parameter estimates are obtained as usual. Return levels are computed thanks to Eq. (3) for return periods ranging from 1 to 100 years. This is repeated a 1000 times.

Confidence bands at 95 % for the return levels of the basic framework (magenta) and the regional framework with three (light blue) and six regions (dark blue) are presented in Fig. 8 and 9 for the high and low risk grid boxes respectively. In addition, to the left of each figure, the smoothed empirical distributions (resulting from the application of the function `density` of `R` to the sample estimates) of the shape (top) and scale parameter (bottom) estimates are shown.

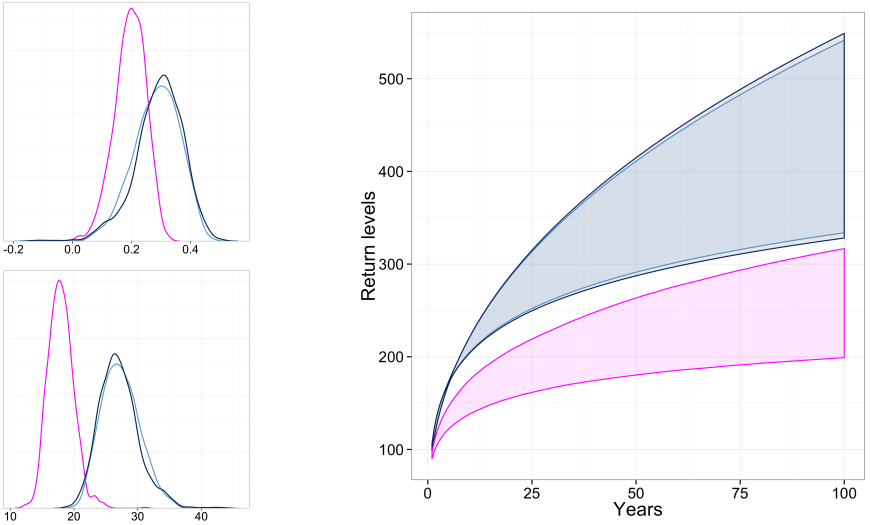

Figure 8: *Uncertainty estimation at the grid box 20 km East of the city of Montpellier (high risk region). Left panel : bootstrap distribution of the shape (top) and scale (bottom) parameters for the basic framework (magenta) and the regional framework with three regions (light blue) and six regions (dark blue). Right panel : 95 % confidence bands for the return level curves with the same color code.*

For the high risk grid box, Fig. 8, the proposed regional framework with either three or six regions tend to yield higher shape and scale parameter estimates which result in significantly higher return levels. In contrast, for the low risk grid box, Fig. 9, the sampling distribution of the shape and scale parameter estimates is similar in both frameworks which explains the overlapping confidence bands of the estimated return levels.

5 Discussion and Conclusion

In an area such as the French Mediterranean area where heavy precipitation events can trigger flash floods with devastating consequences, it is essential to obtain reliable estimates of the distribution of extreme precipitation at both gauged and ungauged locations. To this end, regional analysis can be combined with the block maxima or the peaks-over-threshold approach in a robust framework.

In this paper, we built on the approach proposed in Naveau et al. [2014] to address some of the shortcomings of regional analysis. First, we cast the Naveau et al. [2014] approach into a regional framework for peaks-over-threshold with a single homogeneous region and simplified the expressions to compute the GP parameter estimates. The scaling factor, in this approach, is the estimated

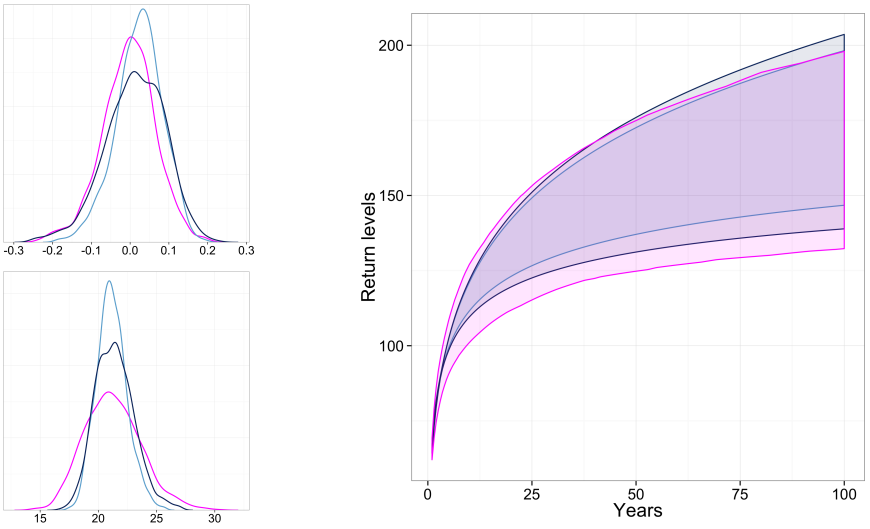

Figure 9: *Uncertainty estimation at the grid box 20 km North of the city of Valence (low risk region). Left panel : bootstrap distribution of the shape (top) and scale (bottom) parameters for the basic framework (magenta) and the regional framework with three regions (light blue) and six regions (dark blue). Right panel : 95 % confidence bands for the return level curves with the same color code.*

conditional expected value of the excesses, noted $\hat{\mu}(\boldsymbol{x}_i)$. Although the scaling factor does not have a clear physical meaning, it does have a clear statistical advantage. Indeed, the scale invariance property of the normalized variable is automatically fulfilled, without further assumptions. In addition, the scale parameter of the normalized variable solely depends on the shape parameter. In other words, in the regional framework proposed in this paper, the regional distribution has a single parameter. Madsen and Rosbjerg [1997] also considered a regional framework for peaks-over-threshold with the expected value of the excesses as the scaling factor. They resorted to L-moment ratios [Hosking and Wallis, 2005] to estimate the shape parameter based on the normalized excesses.

The main contribution of this work is, in the regional framework derived from Naveau et al. [2014], the characterization of homogeneous regions with the second probability weighted moment estimate of the normalized variable, noted $\hat{\nu}(\boldsymbol{x}_i)$ for site i. In the simulation study on synthetic data, homogeneous regions, i.e. with constant shape parameter, were successfully identified. The correct identification of homogeneous regions lead to GP parameter estimates with low variance, as shown by the narrow 95% confidence bands computed with parametric bootstrap. Finally, the use of regressed (as opposed to local) statistics to estimate both μ and ν introduced spatial information and reduced the noise of the estimators. The application on daily precipitation data from the French Mediterranean area illustrated the regional framework on a complex region with several homogeneous sub-regions and shape parameter estimates ranging from approximately 0 to 0.3. For the real data application, uncertainty was estimated with an easy-to-implement spatial block bootstrap. Another approach to properly estimate the uncertainty when observations are spatially dependent has been proposed in Van de Vyver [2012].

As recommended in Hosking and Wallis [2005], most authors (e.g. Kyselỳ et al. [2011]) define regions based on physiographic variables rather than on site statistics. In particular, Hosking and Wallis [2005] argue against the use of the L-CV statistic (L-moment analog of the coefficient of variation). They claim that (1) not much information on homogeneous regions can be gained from the L-CV statistic as it won't take very different values from site to site, (2) outliers might bias the

identification of the regions and (3) the homogeneity of the regions must be tested with a statistic that may contain redundant information with the statistic used to create the regions. We discuss these three points in turn.

(1) The L-CV statistic is used to partition into three homogeneous regions the sites of the French Mediterranean precipitation data in Fig. 10 in order to compare with the partitioning obtains with the ν statistic. The L-CV statistic is estimated at each gauged site with the `R` package `lmomRFA` [Hosking, 2015]. To ensure a fair comparison, the same steps from the regional framework described in Algorithm 1 for the ν statistic are applied : the local L-CV statistics are smoothed with kernel regression, K-Means clusters the sites into three regions and the k-nearest neighbor rule with $k = 5$ assigns each grid point to a region. From Fig. 10, we can see that the L-CV statistic allows to identify the high risk region in the South, including the city of Montpellier. However, the other two regions are not well separated. Similar partitioning are obtained with more regions or with other L-Moment ratios (not shown). This corroborates the claim above that not much information on homogeneous regions can be gained from the L-CV or other L-Moment ratios.

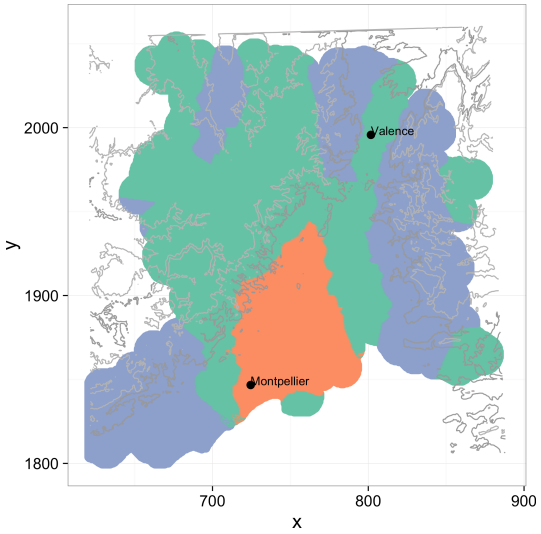

Figure 10: *Partitioning into three homogeneous regions based on the L-CV statistic estimated from kernel regression. K-Means performed the clustering and the k-nearest neighbor rule with $k = 5$ assigned each grid point to a region, following the steps of the regional framework described in Algorithm 1 but with a different statistic.*

On the other hand, in view of the results on both the synthetic and real precipitation data, we claim that the ν statistic is efficient to identify homogeneous regions. The obtained regions are mostly continuous in space and are meaningful according to expert knowledge. The choice of the ν statistic, in the proposed regional framework, is quite natural as it is a summary of the distribution of the normalized variable Z that possesses a unique parameter which is the shape parameter. This is precisely what characterizes homogeneous regions, their shape parameter value. In addition, ν is the lower not trivial probability weighted moment of Z (the only probability weighted moment below ν is the expectation of Z which is one by construction). As each homogeneous region is associated with a shape parameter value derived from the ν statistic, it is associated with an interpretable level of risk of extreme precipitation.

(2) The potential effect of outliers is greatly reduced in the regional framework from Algorithm 1 as the local estimate of ν are regressed. As mentioned earlier, this introduces spatial information and smooths out the noise. Large outliers might still affect the ν estimates but probably to a lesser

degree.

(3) In the proposed regional framework, there is no automated method to select an appropriate number of homogeneous regions. Homogeneity tests could be employed, for instance, to determine if a region needs to be further divided to achieve homogeneity. However, as concluded in Viglione et al. [2007], these tests lack power. For this reason, we prefer to resort to expert knowledge to choose the number of homogeneous regions. This is the only subjective decision in the proposed framework.

Quite often, because its sampling variability is larger than its spatial variability, the shape parameter is kept constant across the region of interest. This appears to be appropriate when studying extremes in a region with little orography such as Belgium [Van de Vyver, 2012]. Nevertheless, in a region with a sharp orography inducing a high spatial variabiliy such as the French Mediterranean area studied in this paper, we believe that the assumption of a constant shape parameter is not realistic. The partitioning into homogeneous regions strikes a middle ground between the assumption of a constant and spatially varying shape parameter. Indeed, each region possesses several sites whose observations contributes to the estimation of the regional shape parameter. In order to guide the selection of the number of homogeneous regions, the sampling distribution could be used to determine how many distinct regional shape parameters can be identified. Preliminary analysis of the French Mediterranean precipitation data showed that at least two regions could be identified. However, this is beyond the scope of this paper and should be further analysed.

Further study is also required in order to determine in which cases the regional framework with the GP distribution proposed in this paper performs better than other interpolation methods such as the direct interpolation of the GP parameters described in the basic framework. For the block maxima approach with the GEV distribution, Carreau et al. [2013] have shown that the regional framework outperforms a direct interpolation of the parameters for sparsely gauged network. In addition, the comparison of return levels showed that there are significant differences between the direct interpolation of the GP parameters from the basic framework and the interpolation from the regional framework for the grid box in the high risk region, see Fig. 8, but not for the grid box in the low risk region, see Fig. 9. Although this should be validated, it might indicate that there is a gain in resorting to the regional framework in particular when the interpolation conditions are more difficult such as when the network is sparsely gauged or when the shape parameter can take high values.

Other perspectives for this work are as follows. Instead of employing the characterization of homogeneous regions to create contiguous regions, the ν statistic could be employed in a region-of-influence type-of approach [Burn, 1990]. Indeed, a neighborhood around a site (gauged or ungauged) could be defined in terms of similarity in the ν statistic. The size of the neighborhood could be determined based on expert knowledge, as for the number of regions in the contiguous case. Another perspective would be to apply the proposed regional framework to a sparsely gauged network. In such a case, covariates would have to be chosen with care. Most likely, x and y coordinates would not be informative enough and covariates related to the orography could be of interest [Benichou and Le Breton, 1987]. In addition, non-parametric methods (k-nearest neighbor rule and kernel regression) worked well in the dense precipitation network to which the regional framework was applied. However, in sparser network, it might be more appropriate to seek parcimonious parametric models.

References

K. M. Abadir and S. Lawford. Optimal asymmetric kernels. *Economics Letters*, 83(1):61–68, 2004.

A. A. Balkema and L. de Haan. Residual life time at great age. *Annals of Probability*, 2(5):792–804, 1974.

P. Benichou and O. Le Breton. Prise en compte de la topographie pour la cartographie des champs pluviometriques statistiques. une application de la methode Aurelhy: la cartographie nationale de champs de normales pluviometriques. *Météorologie*, 1987.

J. Blanchet and M. Lehning. Mapping snow depth return levels: smooth spatial modeling versus station interpolation. *Hydrology and Earth System Sciences*, 14(12):2527–2544, 2010.

M. Borga, E.N. Anagnostou, G. Blöschl, and J.-D. Creutin. Flash flood forecasting, warning and risk management: the HYDRATE project. *Environmental Science & Policy*, 14(7):834 – 844, 2011. ISSN 1462-9011. doi: http://dx.doi.org/10.1016/j.envsci.2011.05.017. URL `http://www.sciencedirect.com/science/article/pii/S1462901111000943`. Adapting to Climate Change: Reducing Water-related Risks in Europe.

I. Braud, P.-A. Ayral, C. Bouvier, F. Branger, G. Delrieu, J. Le Coz, G. Nord, J.-P. Vandervaere, S. Anquetin, M. Adamovic, J. Andrieu, C. Batiot, B. Boudevillain, P. Brunet, J. Carreau, A. Confoland, J.-F. Didon-Lescot, J.-M. Domergue, J. Douvinet, G. Dramais, R. Freydier, S. Gérard, J. Huza, E. Leblois, O. Le Bourgeois, R. Le Boursicaud, P. Marchand, P. Martin, L. Nottale, N. Patris, B. Renard, J.-L. Seidel, J.-D. Taupin, O. Vannier, B. Vincendon, and A. Wijbrans. Multi-scale hydrometeorological observation and modelling for flash flood understanding. *Hydrology and Earth System Sciences*, 18(9):3733–3761, 2014. doi: 10.5194/hess-18-3733-2014. URL `http://www.hydrol-earth-syst-sci.net/18/3733/2014/`.

D.H. Burn. Evaluation of regional flood frequency analysis with a region of influence approach. *Water Resources Research*, 26(10):2257–2265, 1990.

D.H. Burn and N. K. Goel. The formation of groups for regional flood frequency analysis. *Hydrological Sciences Journal*, 45(1):97–112, 2000. doi: 10.1080/02626660009492308. URL `http://dx.doi.org/10.1080/02626660009492308`.

J. Carreau, L. Neppel, P. Arnaud, and P. Cantet. Extreme rainfall analysis at ungauged sites in the South of France: comparison of three approaches. *Journal de la Société Française de Statistique*, 154(2):119–138, 2013.

D. Ceresetti, E. Ursu, J. Carreau, S. Anquetin, J.-D. Creutin, L. Gardes, S. Girard, and G. Molinie. Evaluation of classical spatial-analysis schemes of extreme rainfall. *Natural hazards and earth system sciences*, 12:3229–3240, 2012.

S. Coles. *An Introduction to Statistical Modeling of Extreme Values*. Springer Series in Statistics. Springer, 2001.

D. Cooley, D. Nychka, and P. Naveau. Bayesian spatial modeling of extreme precipitation return levels. *Journal of the American Statistical Association*, 102(479):824–840, 2007.

G. Delrieu, J. Nicol, E. Yates, P.-E. Kirstetter, J.-D. Creutin, S. Anquetin, C. Obled, G.-M. Saulnier, V. Ducrocq, E. Gaume, O. Payrastre, H. Andrieu, P.-A. Ayral, C. Bouvier, L. Neppel, M. Livet, M. Lang, J. P. du Châtelet, A. Walpersdorf, and W. Wobrock. The catastrophic flash-flood event of 8-9 september 2002 in the Gard region, France: A first case study for the Cévennes-Vivarais Mediterranean Hydrometeorological Observatory. *Journal of Hydrometeorology*, 6(1): 34–52, 2005.

J. Diebolt, A. Guillou, and I. Rached. Approximation of the distribution of excesses through a generalized probability-weighted moments method. *Journal of Statistical Planning and Inference*, 137(3):841–857, 2007.

M. Durocher, F. Chebana, and T. B. M. J. Ouarda. Delineation of homogenous regions using hydrological variables predicted by projection pursuit regression. *Hydrology and Earth System Sciences Discussions*, 2016:1–23, 2016. doi: 10.5194/hess-2016-123. URL `http://www.hydrol-earth-syst-sci-discuss.net/hess-2016-123/`.

V. A. Epanechnikov. Non-parametric estimation of a multivariate probability density. *Theory of Probability & Its Applications*, 14(1):153–158, 1969.

A. Ferreira and L. de Haan. On the block maxima method in extreme value theory: PWM estimators. *The Annals of Statistics*, 43(1):276–298, 2015.

R. Fisher and L. H. C. Tippett. Limiting forms of the frequency distribution of the largest and smallest member of a sample. In *Cambridge Philosophical Society*, volume 24, pages 180–190, 1928.

R. Furrer and P. Naveau. Probability weighted moments properties for small samples. *Statistics & probability letters*, 77(2):190–195, 2007.

B. Gnedenko. Sur la distribution limite du terme maximum d'une serie aleatoire. *Annals of mathematics*, pages 423–453, 1943.

V. K. Gupta, O. J. Mesa, and D. R. Dawdy. Multiscaling theory of flood peaks: Regional quantile analysis. *Water Resources Research*, 30(12):3405–3421, 1994. ISSN 1944-7973. doi: 10.1029/94WR01791. URL `http://dx.doi.org/10.1029/94WR01791`.

T. Hayfield and J.S. Racine. Nonparametric econometrics: The np package. *Journal of Statistical Software*, 27(5), 2008. URL `http://www.jstatsoft.org/v27/i05/`.

J. R. M. Hosking and J. R. Wallis. *Regional frequency analysis: an approach based on L-moments*. Cambridge University Press, 2005.

J.R.M. Hosking. *Regional frequency analysis using L-moments*, 2015. URL `http://CRAN.R-project.org/package=lmomRFA`. R package, version 3.0-1.

J. Kyselỳ, J. Picek, and R. Huth. Formation of homogeneous regions for regional frequency analysis of extreme precipitation events in the czech republic. *Studia Geophysica et Geodaetica*, 51(2): 327–344, 2007.

J. Kyselỳ, L. Gaál, and J. Picek. Comparison of regional and at-site approaches to modelling probabilities of heavy precipitation. *International Journal of Climatology*, 31(10):1457–1472, 2011.

Q. Li and J. Racine. Cross-validated local linear nonparametric regression. *Statistica Sinica*, 14 (2):485–512, 2004.

H. Madsen and D. Rosbjerg. The partial duration series method in regional index-flood modeling. *Water Resources Research*, 33(4):737–746, 1997.

E. A. Nadaraya. On estimating regression. *Theory of Probability & Its Applications*, 9(1):141–142, 1964.

P. Naveau, A. Toreti, I. Smith, and E. Xoplaki. A fast nonparametric spatio-temporal regression scheme for generalized Pareto distributed heavy precipitation. *Water Resources Research*, 50(5): 4011–4017, 2014.

J. Pickands. Statistical inference using extreme order statistics. *Annals of Statistics*, 3:119–131, 1975.

B. Renard. A bayesian hierarchical approach to regional frequency analysis. *Water Resources Research*, 47(11), 2011.

B. D. Ripley. *Pattern recognition and neural networks*. Cambridge university press, 1996.

M. Roth, T.A. Buishand, G. Jongbloed, A.M.G. Klein Tank, and J.H. van Zanten. A regional peaks-over-threshold model in a nonstationary climate. *Water Resources Research*, 48(11), 2012.

H. Van de Vyver. Spatial regression models for extreme precipitation in belgium. *Water Resources Research*, 48(9), 2012.

A. Viglione, F. Laio, and P. Claps. A comparison of homogeneity tests for regional frequency analysis. *Water Resources Research*, 43(3), 2007.

G. S. Watson. Smooth regression analysis. *Sankhyā: The Indian Journal of Statistics, Series A*, pages 359–372, 1964.